

# Outer rise seismicity boosted by the Maule 2010 $M_w$ 8.8 megathrust earthquake



Javier A. Ruiz <sup>\*</sup>, Eduardo Contreras-Reyes <sup>1</sup>

Departamento de Geofísica, Facultad de Ciencias Físicas y Matemáticas, Universidad de Chile, Santiago, Chile  
Blanco Encalada 2002, Santiago, Chile

## ARTICLE INFO

### Article history:

Received 9 August 2014  
Received in revised form 7 April 2015  
Accepted 9 April 2015  
Available online 23 April 2015

### Keywords:

Regional moment tensor  
Subduction zone  
Outer rise  
Earthquake cycle  
Oceanic plate

## ABSTRACT

The Maule 2010 megathrust earthquake  $M_w$  8.8 has been characterized by two coseismic high-slip patches (asperities) north and south of the epicenter, separated by a region of lower slip. Here, we invert full broadband waveforms to obtain regional moment tensors, yielding precise centroid depth and source parameters of outer rise events ( $M_w > 4.5$ ), including a large  $M_w$  7.4 event that occurred just 1.5 h after the Maule mainshock. Outer rise seismicity occurred mainly in two clusters: (1) a large number of outer rise events in the subducting plate located just seaward of the northern asperity of the Maule earthquake, and (2) a second cluster with fewer events seaward of the southern edge of the Maule rupture area. Thus, the outer rise seismicity is correlated with the coseismic rupture of the Maule earthquake, reflecting the stress state of the interplate coupled zone. The moment tensor results indicate similar extensional focal mechanisms for all outer rise events in the northern zone. In the southern region, most of the outer rise events are also extensional, except for one strike slip event located near the oceanic Mocha Fracture Zone. The centroid depths vary from 5 to 20 km depth, and present similar magnitudes. Many of the outer rise events nucleated near the Mocha Fracture Zone, including the  $M_w$  7.4 event and one strike-slip event. The calculated yield strength envelope for the oceanic Nazca lithosphere suggests that the centroid depths of intraplate tensional events span almost the entire upper-brittle part of the oceanic lithosphere.

© 2015 Elsevier B.V. All rights reserved.

## 1. Introduction

The outer rise, or outer trench slope, is a broad, gentle upwarping of the seafloor where an incoming/subducting oceanic plate begins to flex and descends into the trench. Large extensional earthquakes within the outer rise of the subducting plate are rare compared to large interplate thrust events on the subduction interface. Although some large extensional faulting events, such as the 1977 Sumbawa, Indonesia,  $M_w$  8.4 (Spence, 1986) and 2009 Samoa–Tonga  $M_w$  8.1 (Lay et al., 2010) earthquakes, do not follow soon after plate boundary thrust events, may do [for example, the 1933 Sanriku–Oki,  $M_w$  8.6 (Kanamori, 1971) and the 2007 Kuril  $M_w$  8.1 (Ammon et al., 2008) earthquakes]. Studies conducted on outer rise seismicity suggest that it is strongly correlated with spatial and temporal variations of the seismic coupling along megathrust, reflecting the stress state of the interplate coupled zone (e.g. Christensen and Ruff, 1988). These events are not only mechanically, but also spatially and temporally, related to the distribution of large thrust earthquakes, and are thus an integral part of the earthquake cycle.

Outer rise seismicity along subduction zones occurs mainly at shallow depths (<30 km) within the oceanic plate with normal faulting mechanisms; deeper events are less common (e.g. Christensen and Ruff, 1988). The focal depth variation and faulting type are usually explained by elastic stresses within the subducting slab that undergoes bending. Some basic models (e.g. Chapple and Forsyth, 1979) consider a bending elastic plate, which results in tensional stress in the upper part of the plate and compressional stress in the lower part of the plate. These stress regimes are separated at some depth by a neutral plane. Statistical studies of outer-rise intraplate events suggest that the transition depth from tensional to compressional stress regimes within the subducting oceanic lithosphere is located approximately at the depth of the 400 °C–450 °C isotherm (e.g. Seno and Yamanaka, 1996).

The spatial and temporal occurrence of outer rise events can also be explained by stress fluctuations related to megathrust earthquake cycles, based on simulation of great earthquakes with mechanical models (e.g. Dmowska et al., 1988; Taylor et al., 1996; Dmowska et al., 1996). In particular, model simulations show extensional outer rise earthquakes and compressional ones in the early and late phase of the megathrust earthquake cycle, respectively, which agrees rather well with seismicity observations from coupled subduction zones (e.g. Dmowska et al., 1988). For instance, Christensen and Ruff (1988) argued that tensional outer rise events follow large underthrusting earthquakes in strongly

<sup>\*</sup> Corresponding author at: Departamento de Geofísica Facultad de Ciencias Físicas y Matemáticas Universidad de Chile Blanco Encalada 2002, Santiago, Chile. Tel.: +56 2 2978 0690; fax: +56 2 2696 8686.

<sup>1</sup> Tel.: +56 2 2978 0690; fax: +56 2 2696 8686.

coupled zones, whereas compressional outer rise earthquakes are triggered seaward of locked sections of the interplate zone. On the other hand, the same authors have proposed that in weakly-coupled subduction zones, only tensional outer rise earthquakes occur, which indicates that the outer rise is dominated by tensional stresses associated with plate bending stresses and/or slab pull forces.

On February 27, 2010, an  $M_w$  8.8 mega-thrust earthquake nucleated at 06:34:08 UTC, with a hypocenter located at 73.239°S, 36.290°W and 30 km depth, according to the Servicio Sismológico Nacional (SSN) of the Universidad de Chile. This earthquake broke an approximately 450-km long segment of the south-central Chile subduction zone (e.g. Delouis et al., 2010; Moreno et al., 2012; Vigny et al., 2011). A devastating tsunami followed this event (e.g. Fritz et al., 2011; Vargas et al., 2011). Preceding the Maule 2010 earthquake, the south-central Chilean subduction zone had been identified as a likely mature seismic gap (Madariaga et al., 2010; Ruegg et al., 2009) because no large subduction earthquake had occurred in this zone since 1835. The coseismic slip imaged by several groups (e.g. Delouis et al., 2010; Lorito et al., 2011; Moreno et al., 2012; Vigny et al., 2011; Hayes et al., 2013) shows similar large-scale spatial slip patterns in the rupture area. Most of the published co-seismic slip models show two patches of large slip with the largest slip located north of the epicenter. The rupture propagated predominantly bilaterally, but most of the seismic moment occurred in the northern rupture area, with peak slip on the order of 15–20 m. The total seismic moment was about  $1.8\text{--}2.6 \times 10^{22}$  N·m (e.g. Delouis et al., 2010; Hayes et al., 2013).

Intense aftershock activity followed the 2010 Maule earthquake, and the spatial distribution of the seismicity has been located and analyzed by few groups. Characteristic features include a shallow concentration of events between 10 and 35 km depth and a group of deeper events lying at 40–50 km depth (e.g. Hayes et al., 2013; Lange et al., 2012; Rietbrock et al., 2012). Despite the diverse focal mechanisms and magnitudes, most of the aftershock seismicity was located in the northern part of the rupture area. Also shallow intraplate coastal events were triggered at the northern edge of the rupture zone (e.g. Farías et al., 2011; Lange et al., 2012) and two large normal faulting earthquakes occurred near Pichilemu (~34°S) on March 11, 2010, with magnitudes  $M_w$  7.0 and  $M_w$  6.9 (Ruiz et al., 2014; Ryder et al., 2012).

In the oceanic plate, outer rise seismic activity following the 2010 Maule earthquake was distributed spatially in two main areas. To the north (~34.5°S), outer rise events were distributed at the outer trench slope zone adjacent to the northern largest coseismic slip patch. A second cluster of outer rise seismicity was concentrated at ~38°S, seaward of the southern edge of the Maule rupture area (Moscoso and Contreras-Reyes, 2012). A large  $M_w$  7.4 outer rise normal faulting event occurred just 1.5 h after the great  $M_w$  8.8 Maule earthquake and was reported by some seismological agencies, such as, GCMT (Global Centroid-Moment-Tensor, <http://www.globalcmt.org/>) and NEIC (National Earthquake Information Center). For instance, NEIC estimated the origin time of the event at 08:01:23 UTC and located it beneath the outer trench slope zone with an epicenter at 37.773°S, 75.048°W and a depth of 35 km. Similar large outer rise aftershocks followed the 2011,  $M_w$  9.1, Tohoku megathrust earthquake, along the subduction zone in Japan, where about 40 min after the mainshock, an  $M_w$  7.6 earthquake occurred beneath the outer trench slope (e.g. Asano et al., 2011; Lay et al., 2011; Obana et al., 2012). These earthquakes reflect the tensional stresses that take place in the outer rise zone after a megathrust earthquake, and the fluctuation of the stress–strain transferred from coseismic thrust earthquake ruptures may play an important role in the occurrence of large normal faulting earthquakes.

Another remarkable seismic event triggered by a megathrust earthquake is the intraplate event of April 2012 off Sumatra,  $M_w$  8.6. This is the largest strike–slip and intraplate earthquake ever recorded, and it had a complex rupture and was followed approximately 2 h later by a strike–slip  $M_w$  8.2 aftershock (e.g. Yue et al., 2012). These events occurred ~7 years after the 2004 Sumatra–Andaman megathrust

earthquake  $M_w$  9.2. The 2012 intraplate seismicity occurred along the fossil fabric of the extinct Wharton basin off Sumatra, and according to coseismic slip and Coloumb stress change calculations and seismological studies, before the April 2012 and after the Sumatra events there was virtually no seismicity along the Wharton basin (Delescluse et al., 2012; Meng et al., 2012). The Nazca plate of central Chile hosted a prominent oceanic fracture zone: the Mocha Fracture Zone (FZ) that trends N55°E, and is currently subducting at ~38°S (Contreras-Reyes et al., 2008). In this paper, we also explore and discuss possible reactivation of this fossil transform fault in terms of the stress transfer triggered by the Maule megathrust earthquake.

The main aim of this study is to characterize earthquake source parameters of the outer rise seismicity following the 2010  $M_w$  8.8 Maule earthquake by modeling regional seismic moment tensors to better determine precise centroid source depths, and to relate them to the megathrust zone and surrounding areas. We invert the waveforms to obtain regional moment tensors and we compute the best source depth for a large dataset ( $M > 4.5$ ) of outer rise events compared to those reported by seismological agencies using teleseismic data. Because the largest  $M_w$  7.4 outer trench slope earthquake was triggered about 1.5 h after the mainshock, waveforms are affected by seismic waves from the mainshock. Consequently an accurate seismic-to-noise ratio analysis was done prior to running the inversion. Finally, we discuss the interplay between the outer rise seismicity and the coseismic slip distribution of the 2010 megathrust earthquake in terms of the geodynamic setting of the incoming oceanic Nazca plate.

## 2. Seismotectonic setting

The study area spans from 32°S to 39°S along the south-central Chilean subduction zone, where the oceanic Nazca plate subducts beneath South America in a N78°E direction with a converge rate of about 6.7 cm/year (Khazaradze and Klotz, 2003). In the study area, the seafloor spreading fabric of the oceanic Nazca plate trends oblique to the trench axis. However, the seafloor spreading fabric is perturbed/modified in the outer rise region due to existence of cross-cutting normal faults caused by plate bending (e.g. Contreras-Reyes et al., 2008; Moscoso and Contreras-Reyes, 2012). The study area is bounded by the presence of two prominent bathymetric features: the Juan Fernández Ridge (JFR) and the oceanic Mocha FZ in the north and south, respectively (Fig. 1). North of the Mocha FZ, the plate age at the trench axis is ~30 Ma, whereas south of it the seafloor is about 24 Ma (Tebbens et al., 1997).

The 2010,  $M_w$  8.8, Maule earthquake broke a previously identified seismic gap in the zone (Ruegg et al., 2009) that had not ruptured since 1835. The 1835 event, summarized by Charles Darwin, had an estimated magnitude of about  $M$  8.5 (Lomnitz, 2004). Hayes et al. (2013) analyzed the aftershock sequence of the Maule earthquake and found that most of the aftershocks are interplate thrust events located away from regions of largest coseismic slip; they also identified clusters of seismic events located in the oceanic plate at the ends of the main rupture area, implying internal deformation of the subducting slab in response to a large amount of slip on the plate interface.

Outer rise seismicity in the study area since 1976 and prior to the Maule earthquake is summarized in Fig. 1A. Events ( $M > 4.0$ ) were downloaded from NEIC (<http://earthquake.usgs.gov/neic>). We selected those with epicenters located westward of the trench axis. Using the same location criteria, centroid moment tensors ( $M > 5.0$ ) from GCMT were selected in the same region. Noting that both datasets may present uncertainties in hypocenter and centroid locations, some events may not correspond to outer rise events. Nonetheless, one can observe three clusters of events located at the northern (~33°S) and southern parts of the study area (~39°S). The region seaward of Valparaíso experienced two large outer rise events, in 1981 and 2001. The 1981,  $M_s$  7.2, was a compressional event with a source depth of 30 km (Korrat and Madariaga, 1986) which occurred south of Juan Fernandez Ridge

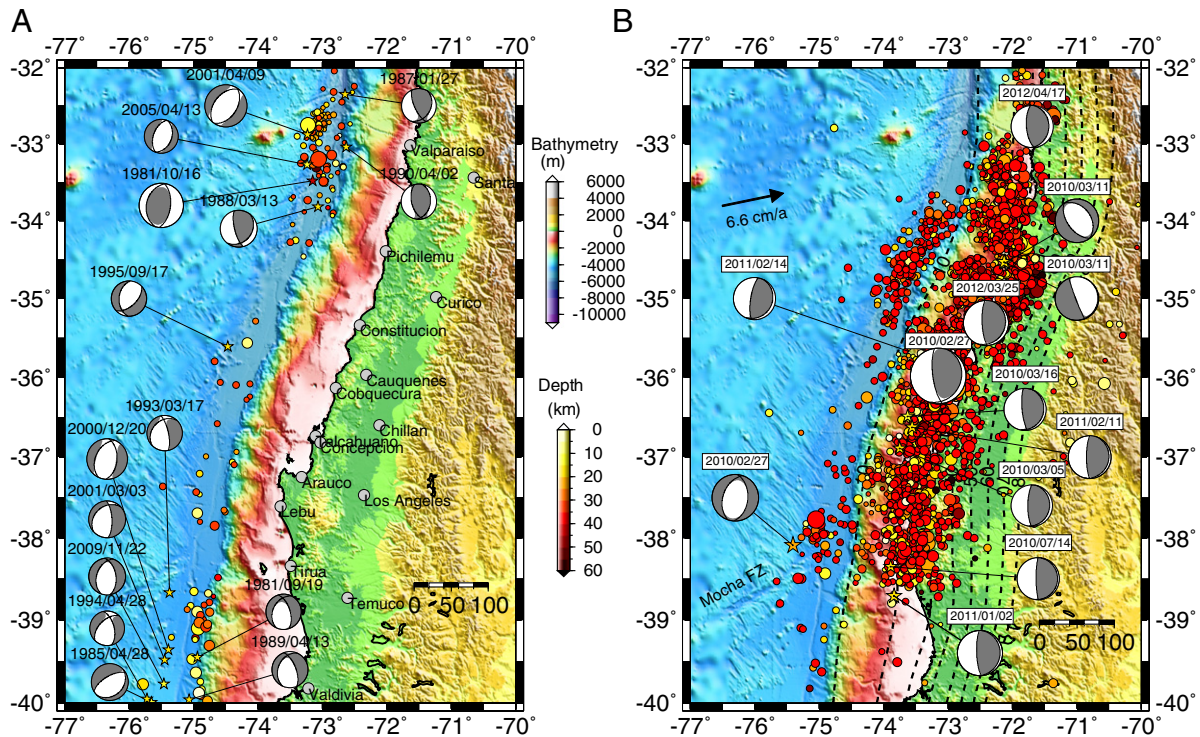


**Fig. 1.** Bathymetric/topographic map and seismicity of the study area. (A) Outer rise seismicity ( $M > 4.0$ , from NEIC catalog) located since 1976 and prior to the 2010,  $M_w$  8.8, Maule earthquake. Beach balls are the centroid moment tensors from GCMT catalog for events  $M > 5.0$ . (B) Seismicity reported by NEIC after the Maule earthquake in the period 27-02-2010 to 31-12-2013. Colored circles are aftershocks with sizes scaled to the event magnitude and the colorbar represents hypocenter depths. Beach balls correspond to global centroid moment tensors for the largest aftershocks ( $M_w > 6.5$ ) recorded after the 2010 Maule earthquake. Dashed black lines are the contour depth (every 10 km) of the subducting oceanic slab (from Slab1.0, Hayes et al., 2013).

(JFR). In contrast, an extensional event triggered at 12 km depth northward from the 1981 event, with a magnitude  $M_w$  7.0 that occurred on April 9, 2001 (Clouard et al., 2007). Both events were followed by several aftershocks, and from centroid moment tensor solutions reported by GCMT, the 1990,  $M_w$  5.6, event had similar focal mechanism as the 1981 outer rise event. In 2005, an event  $M_w$  5.4 with similar mechanism to the 2001,  $M_w$  7.0, event was reported by the GCMT.

All the southern outer rise events show similar extensional faulting mechanisms according to the GCMT (Fig. 1A). Outer rise seismicity is distributed along a narrow north–south strip from  $\sim 38.5^\circ\text{S}$  to  $40^\circ\text{S}$ , and among these events eight present extensional focal mechanisms with strike predominantly parallel to the trench axis according to the moment tensor solutions of the GCMT. The largest event occurred in December 20th, 2000, with a centroid depth at 15 km and magnitude  $M_w$  6.4 according to GCMT.

Fig. 1B summarizes the spatial distribution of aftershocks ( $M > 4.0$ ) that occurred after the 2010 Maule earthquake, located by the NEIC. The centroid moment tensors of the largest aftershocks ( $M_w > 6.5$ ) reported by the GCMT reveal the diversity of earthquake faulting in the aftershock sequence. In particular, a large  $M_w$  7.4 outer trench slope earthquake occurred seaward at the southern edge of the main rupture area ( $\sim 38^\circ\text{S}$ ). Most of the outer rise events occurred at the northern and southernmost regions of the Maule 2010 rupture area. Little outer rise activity occurred in the middle just seawards of the epicentral region. The northern zone runs approximately from  $33.5^\circ\text{S}$  to  $35.5^\circ\text{S}$ , and it presents a larger density of seismicity compared to the southern cluster located from  $37.5^\circ\text{S}$  to  $38.5^\circ\text{S}$ . Most of the later events are presumably aftershocks of the  $M_w$  7.4 outer rise earthquake (Fig. 1).

Nevertheless, the southern outer rise seismic sequence is highly remarkable in terms of the largest magnitude  $M_w$  7.4 event triggered and its proximity to the Mocha FZ. This event occurred as a direct response to the mainshock, and is the largest outer rise event instrumentally reported along the Chilean subduction zone; the  $M_w$  7.0 that

occurred westward off Valparaiso in 2001 is the second largest (Clouard et al., 2007). Fig. 2 shows the centroid moment tensor of the  $M_w$  7.4 event and the aftershocks following this event reported by the NEIC ( $M > 4$ ). We also show the centroid moment tensor solutions computed by the GCMT ( $M > 5.0$ ). Five events, including the  $M_w$  7.4, correspond to normal faulting with nodal planes striking nearly parallel to the trench axis, except for one event striking obliquely to the trench axis. Also a strike slip event was triggered in the outer trench slope zone near the Mocha FZ. Outer rise seismicity located by NEIC shows a spatial distribution that is elongated north–south. Focal depths vary between 5 and 35 km, however, several events are located at 35 km depth, meaning that the hypocenter depth is poorly constrained. Likely, these events have large depth uncertainties, as is typical when locating earthquakes at teleseismic distances.

For events with magnitudes usually larger than 4.5 – depending on signal-to-noise ratio of records – it is possible to compute regional seismic moment tensors and to more precisely determine the centroid depth by iterating the inversion process over several source depths to search for the best fitting model (e.g. Dreger, 2003; Kubo et al., 2002; Pasyanos et al., 1996; Ritsema and Lay, 1995). In the next section, we present the inversion of regional moment tensors from seismological recordings for the sequence of outer rise events.

### 3. Data, analysis, modeling and testing

#### 3.1. Data set

We selected from the NEIC worldwide catalog events with  $M > 4.5$ , located in the outer rise region along south-central Chile, including 3 years from February 27, 2010. For each event in this dataset, we downloaded 3-component broadband waveforms for all stations located at regional distances ( $\Delta < 12^\circ$ ) from the NEIC online web facilities. Digital broadband recordings were available through the Global

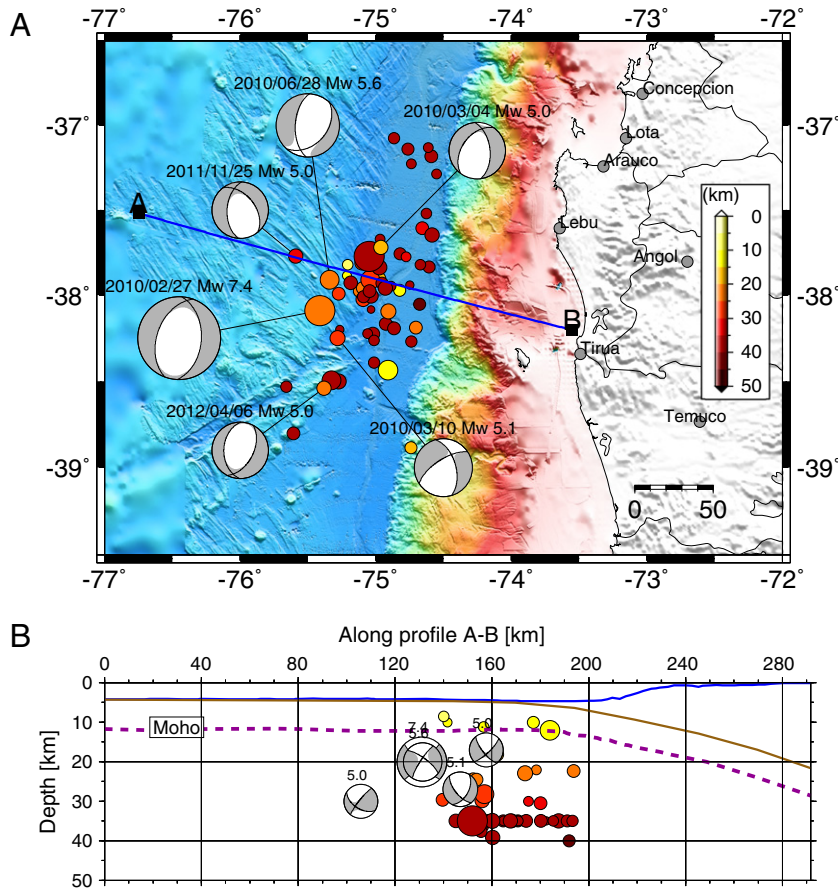


**Fig. 2.** (A) High resolution bathymetric map (Contreras-Reyes et al., 2008). Seismicity and source mechanism for the outer rise events occurred at 38°S of the study area. Colored circles are events located by the NEIC in the period 27-02-2010 to 31-12-2013, with their sizes scaled to magnitude. Colorbar represents hypocenter depths. Beach balls are centroid moment tensor solutions by the GCMT for events with magnitude  $M_w > 5.0$ . (B) Cross-section A–B shows the centroid depth by GCMT solutions (beach ball) and colored circles are hypocenter depths by NEIC. Brown line is the top of the oceanic subducting slab, purple dashed line is the Moho discontinuity and the blue solid line is the bathymetry taken from the 2D seismic tomography model by Contreras-Reyes et al. (2008).

Seismographic Network (GSS), and the Incorporated Research Institutions for Seismology (IRIS) Data Management Center.

### 3.2. Inverse method for regional moment tensors

We used the Time-Domain Moment Tensor (TDMT) inverse code to retrieve the seismic moment tensor from broadband regional waveform records (e.g. Dreger, 2003; Fukuyama and Dreger, 2000; Pasyanos et al., 1996). This software package has been used routinely at the University of California, Berkeley Seismological Laboratory, and successfully implemented at the Japan National Research Institute for Earth Sciences and Disaster Prevention (NIED). This method solves a linear inverse problem to retrieve deviatoric seismic moment tensors from full regional broadband records in the time domain via a linear least square algorithm. For a given source depth, the inversion scheme computes the best fitting RMS (root mean square) or largest variance reduction (VR), of deconvolved data and synthetic waveforms filtered in a common frequency band.

The misfit error between synthetics and observed waveforms is simply evaluated with the variance reduction (VR) defined by,

$$VR = \left[ 1 - \sum_i \left( \frac{\sqrt{(o_i - s_i)^2}}{\sqrt{o_i^2}} \right) \right] \times 100 \quad (1)$$

$s_i$  and  $o_i$  are the synthetic and observed waveforms, respectively and where sum is over stations and components. The best centroid depth is computed iteratively every 2 km depth by finding the solution that

yields the largest variance reduction over a broad depth range, or equivalent to the minimum Chi-square statistic. The best final seismic moment tensor is expressed as a percentage of pure double-couple (DC) and percentage of compensated linear vector dipole (CLVD) moment tensors, and nodal planes are computed from DC. In this approach we assume purely deviatoric seismic moment tensors, so we do not invert for the isotropic (ISO) part of the moment tensor.

Green's functions are computed for a 1D velocity crustal model using a frequency–wavenumber integration method (Saikia, 1994). The 1D velocity model used in this study corresponds to the one proposed by Campos et al. (2002) which is a crustal model representative for south-central Chile. This velocity model provides reasonable solutions for regional moment tensors, even if the earthquake source is located in the outer rise, because the regional broadband waveforms inverted in this study and recorded at stations installed on land correspond mainly to surface waves propagating predominantly through the continental crust. The epicenter location reported by the NEIC was fixed and a point-source was assumed for the regional events investigated in this study, which is good assumption for the moderate to large events ( $M_w < 7.5$ ) and the frequency band in which these events are analyzed.

### 3.3. Data selection and processing

Before running the moment tensor inversion, we performed signal-to-noise ratio analyses for the dataset in order to check if the frequency band used in the inversion covers a band with good signal-to-noise ratios. It is important to check the noise level at far stations and for events with small magnitudes (of about  $M_w < 5.0$ ), but also particularly

needed for the records of the 2010,  $M_w$  7.4, outer-rise event. In the latter case, broadband recordings may present saturation at close stations, and/or be noisier than expected because seismic waves radiated from the 2010,  $M_w$  8.8, Maule earthquake overlap with those from the source of the outer rise event.

Fig. 3 shows the 3-component broadband recordings at station TRQA for the  $M_w$  7.4 event; instrument response was deconvolved and the waveform was integrated once to yield the displacement signal. The unfiltered records present a very long period wave (Fig. 3A) that appears more evident at the coda. Waveforms were bandpass filtered in the frequency band 0.008–0.035 Hz prior to inversion. Fig. 3B shows the bandpass filtered waveforms used in the inversion. The 3-component of the bandpass filtered displacement show a good quality in terms of surface waves amplitudes radiated by the earthquake. The O marker corresponds to the origin time of the event estimated by the NEIC. Fig. 3C shows a comparison of the Fourier spectrum amplitudes of the waveform portion of the signal used in the inversion and the seismic noise extracted before the P-wave arrival time. The spectral amplitudes in the frequency range 0.008–0.035 Hz indicate that the signal is stronger than the noise in this band for the  $M_w$  7.4 event.

### 3.4. Robustness

The  $M_w$  7.4 outer rise event was well recorded at regional distances, but some stations did saturate. At teleseismic distances, records are much noisier because seismic waves from the  $M_w$  7.4 and  $M_w$  8.8 earthquakes overlap each other. The regional stations present reasonable azimuthal coverage onshore (Fig. 4A). We removed the instrument response, rotated to the great-circle path, integrated velocities to obtain displacements, and applied a bandpass filter to synthetic and observed seismograms prior to running the inversion. A causal 4th pole Butterworth bandpass filter was applied in the frequency band that depends on the magnitude (Kubo et al., 2002). For the largest

event,  $M_w$  7.4, we slightly modified the frequency band proposed by Kubo et al. (2002) to the one used in this study, 0.008–0.035 Hz, because of the overlapping issue discussed previously. However, for the remainder of the events we applied the frequency band magnitude-dependent filter suggested by Kubo et al. (2002). The last frequency bands correspond to the ones routinely and broadly used in real time seismic monitoring to invert regional moment tensors in Japan, for instance.

Fig. 4B shows the inversion result for one event, where the variance reduction and moment tensor solution is shown as a function of source depth, the best solution is retrieved at 16 km depth that gives the largest variance reduction, which is representative of the centroid depth of the event at the epicenter location. The 3-component waveform that fits for all stations used in the inversion are shown in Fig. 4C for the best-fitting depth. The synthetic waveforms fit rather well the observed ones, with a VR = 80%. The scalar seismic moment,  $M_0$  is  $1.23 \times 10^{21}$  N·m, with  $M_w = 7.4$ . The percentages of DC and CLVD are 62% and 38%, respectively. The nodal planes are,  $5^\circ/55^\circ/-104^\circ$  and  $208^\circ/38^\circ/-72^\circ$  (strike/dip/rake), showing a normal sense of faulting for this outer rise event. This solution agrees rather well with the centroid moment tensor solution published by the GCMT [ $M_0 = 1.36 \times 10^{21}$  N·m,  $M_w = 7.4$ , 20 km centroid depth and nodal planes given by,  $3^\circ/46^\circ/-102^\circ$ , and  $200^\circ/46^\circ/-78^\circ$  (strike/dip/rake)].

Next, we selected outer rise GCMT events and inverted for their regional moment tensors following the methodology described in this study. Fig. 5A shows the comparison of the solutions obtained in this study and those computed by the GCTM. The faulting mechanism agrees rather well among events, and some minor differences appear, but are in the order of the expected error range for these kind of inverse methods, which are approximately  $\pm 20^\circ$  (e.g. Hayes et al., 2013). However, inverting for regional moment tensors from broadband data allows one to better constrain centroid depths, compared to methodologies using teleseismic data. The centroid depths from GCMT tend to be predominantly deeper than best source depths estimated in this study (Fig. 5B). Also, the spatial location of outer rise events shown in Fig. 5A can differ because we used the epicenter location determined by the NEIC, instead of centroid locations provided by the GCMT.

## 4. Results

Similar methodology was applied to the whole set of events selected in the outer rise region of the Maule rupture area. The seismic-to-noise ratio analyses conducted on broadband records allowed us to derive moment tensors for a total of 28 events, listed in Table 1, for the southern events, and Table 2, for northern events. Both tables summarize event location, origin time, nodal planes, scalar seismic moment, magnitude, and the percentage of DC and CLVD. We also include the variance reduction and the number of stations used in the inversion.

For the study area and time period selected for this work, the GCMT reported a total of 14 centroid moment tensors for events in the outer rise. We analyzed a total of 29 events, including the  $M_w$  7.4 earthquake.

The source mechanism of southern outer rise events present normal faulting, and some of them can be associated as aftershocks of the  $M_w$  7.4 outer trench slope earthquake (Fig. 6A). Most of the events have a strike similar to the strike of the  $M_w$  7.4 and are closely parallel to the trench, and the rest of events are obliquely oriented with respect to the trench axis. From the best double-couple solutions, the majority of events strike nearly parallel to the trench axis, except four events that in average strike N20°W. The diversity of faulting mechanisms retrieved can be associated with the proximity to the Mocha FZ in the outer rise region. A strike slip event was triggered, and we suspect may be associated with, a pre-existing complex fault system near the Mocha FZ. Also note that the possible reactivation of the Mocha FZ landwards of the trench has been already pointed out by Lange et al. (2012).

In terms of centroid depths, all events are shallower than the  $M_w$  7.4 event, and located above the neutral plane (~20 km depth) that delimits

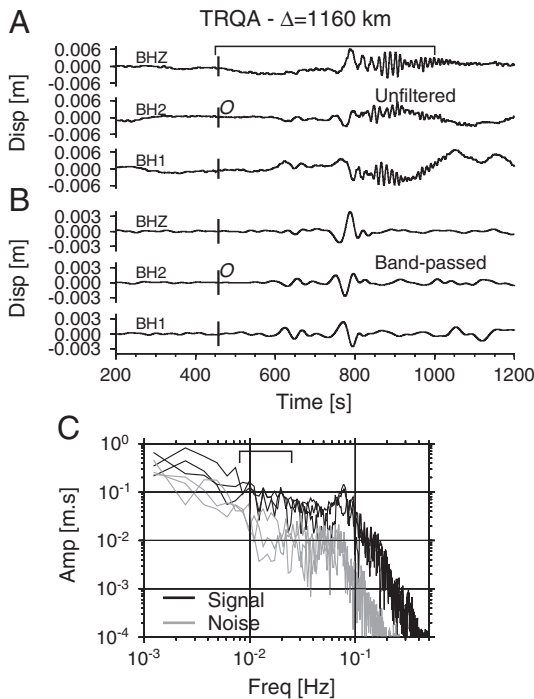
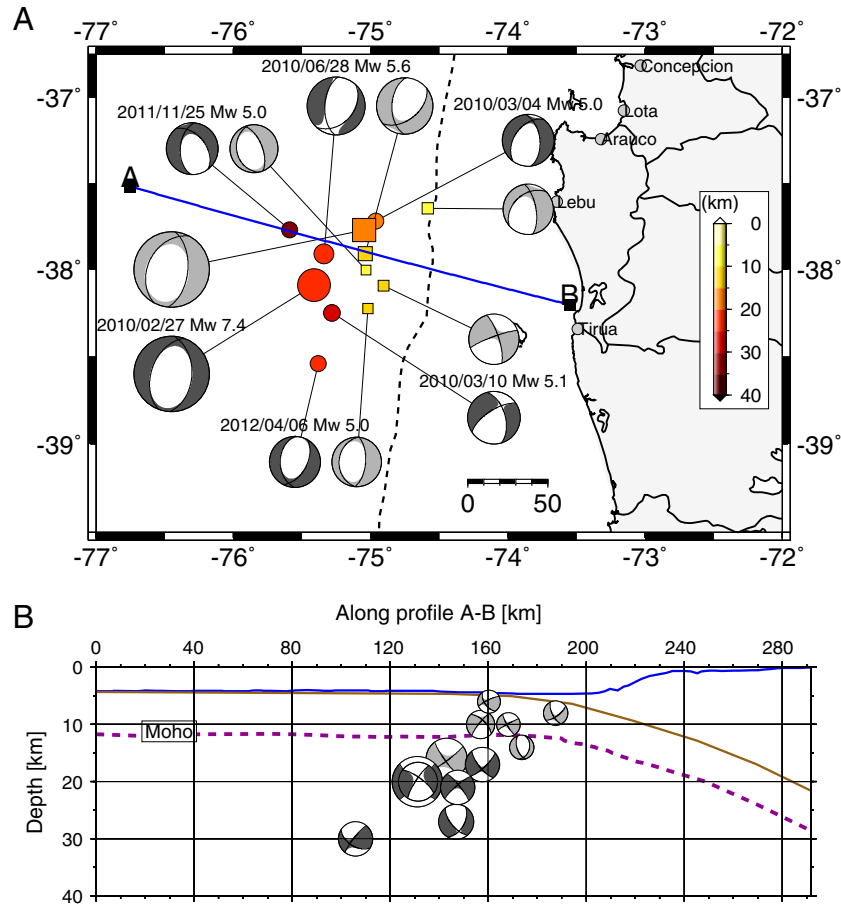


Fig. 3. Signal-to-noise ratio analysis performed on broadband records of the 2010,  $M_w$  7.4, outer trench slope earthquake, three components, recorded at TRQA station. (A) Unfiltered displacements with instrument response removed. (B) Displacement filtered in the bandpass 0.008–0.035 Hz. (C) Comparison of the Fourier spectrum amplitudes of noise and signal extracted from the unfiltered waveforms. The O marker is the origin time reported by NEIC. The upper bracketed line at the top of each panel delimits the time window and the frequency band used in the inversion.





**Fig. 5.** Comparison of seismic moment tensors reported by the GCMT (dark gray) and the ones computed in this study (light gray). (A) Map view of the centroid (GCMT, colored circles) and epicenter (NEIC, colored squares) locations. Dashed line is the trench axis, and color bar represents centroid and hypocenter depths. (B) Cross-section A–B shows the centroid and best source depth estimated by GCMT and this study, respectively. Brown line presents the top of the oceanic subduction slab, purple dashed line is the Moho discontinuity and the blue solid line is the bathymetry (after Contreras-Reyes et al., 2008).

### 5. Discussion

#### 5.1. Methodology and seismological results

The comparison of our regional moment tensor solutions against the GCMT solutions supports the reliability of our analysis and the reasonable solutions for the source mechanism. However, the regional

moment tensors provide better estimate of centroid depths as shown in this study for moderate magnitude events. The centroid depths obtained for both outer rise clusters are consistent with the mechanical behavior of the oceanic subduction slab subjects to bending in the outer rise zone. However, at regional distances and for off-shore events the azimuth coverage is a permanent limitation when having oceanic-continental subduction zone margin, thus it is needed to use at least

**Table 1**

Earthquake source parameters and focal mechanisms for the outer rise events triggered in the southern zone of the Maule rupture area. NP1 and NP2 are nodal planes (strike/dip/rake), VR, variance reduction, DC, percentage of double-couple, CLVD, percentage of compensated linear vector dipole, and NST number of stations used in the inversion.

	Date	Time [UTC]	Lon [°]	Lat [°]	Depth [km]	M <sub>0</sub> [Dyne.cm]	M <sub>w</sub>	NP1	NP2	VR	DC	CLVD	NST
Main	27-02-2010	8:01:21	-75.048	-37.773	16	1,23E + 30	7.40	5/55/-104	208/38/-72	79	62	38	6
1	28-02-2010	10:43:07	-75.273	-38.501	16	3,13E + 26	5.00	43/58/-88	219/32/-93	49	20	80	3
2	01-03-2010	6:16:06	-74.928	-37.958	14	8,85E + 25	4.60	39/65/-93	227/25/-83	70	72	28	2
3	01-03-2010	8:58:32	-74.740	-37.850	12	3,09E + 26	5.00	31/63/-83	196/27/-103	75	64	36	3
4	04-03-2010	9:03:37	-74.582	-37.647	8	2,99E + 26	5.00	350/66/-125	229/41/-38	81	72	28	3
5	10-03-2010	16:00:51	-74.906	-38.093	14	2,75E + 26	4.90	250/82/-15	342/75/-172	70	86	14	3
6	20-03-2010	5:39:26	-74.863	-38.192	10	1,08E + 26	4.70	348/68/-100	193/24/-67	78	89	11	3
7	28-06-2010	0:59:46	-75.038	-37.910	10	2,11E + 27	5.50	183/52/-124	51/49/-54	77	79	21	4
8	25-11-2011	17:35:44	-75.032	-38.003	6	1,26E + 26	4.70	338/62/-95	168/29/-81	78	71	29	4
9	28-12-2011	19:54:24	-75.060	-37.941	8	1,08E + 26	4.70	15/63/-82	179/28/-105	81	68	32	3
10	06-01-2012	8:08:37	-75.091	-38.024	8	6,37E + 25	4.50	358/61/-89	175/29/-93	76	80	20	3
11	07-02-2012	12:02:11	-74.974	-37.902	8	7,41E + 25	4.50	1/61/-89	179/29/-92	80	74	26	4
12	06-04-2012	13:25:03	-75.019	-38.226	10	2,07E + 26	4.80	4/61/-91	186/29/-88	81	74	26	3
13	15-06-2012	5:43:11	-74.702	-38.188	6	8,48E + 25	4.60	347/61/-96	179/30/-79	80	80	20	4
14	24-08-2013	7:00:17	-75.272	-37.991	6	6,78E + 25	4.50	330/64/-96	164/26/-77	85	86	14	3
15	21-10-2013	18:17:21	-75.100	-37.809	8	2,78E + 26	4.90	15/59/-87	190/31/-94	80	69	31	5

**Table 2**  
Same as Table 1, for outer rise events triggered in the northern zone of the study area.

	Date	Time [UTC]	Lon [°]	Lat [°]	Depth [km]	$M_0$ [Dyne.cm]	$M_w$	NP1	NP2	VR	DC	CLVD	NST
1	28-02-2010	1:45:29	-73.689	-34.450	12	7,45E + 26	5.20	45/60/-89	222/30/-92	67	65	35	4
2	28-02-2010	14:50:32	-73.287	-33.894	8	2,15E + 26	4.90	45/58/-85	216/32/-97	64	97	3	4
3	01-03-2010	5:30:35	-73.596	-34.674	8	1,79E + 26	4.80	40/55/-102	241/37/-73	56	77	23	5
4	01-03-2010	12:20:18	-73.736	-34.537	8	4,69E + 26	5.10	40/56/-96	231/35/-81	67	68	32	4
5	01-03-2010	14:36:30	-73.504	-34.390	8	6,35E + 26	5.20	44/55/-97	236/36/-80	60	65	35	4
6	01-03-2010	22:40:18	-73.814	-34.831	10	2,31E + 26	4.90	32/61/-98	228/30/-76	65	65	35	4
7	02-03-2010	9:44:56	-73.347	-34.162	10	1,39E + 26	4.70	40/63/-87	214/28/-95	70	91	9	4
8	08-03-2010	13:03:43	-73.820	-34.533	8	5,21E + 26	5.10	44/57/-93	229/34/-86	70	70	30	5
9	09-03-2010	21:59:23	-73.949	-34.765	12	1,51E + 26	4.80	24/54/-96	213/36/-82	68	90	10	4
10	10-03-2010	8:45:22	-73.831	-34.992	8	2,47E + 26	4.90	37/54/-91	218/36/-89	76	90	10	4
11	23-03-2010	3:44:58	-73.820	-34.808	10	1,39E + 26	4.70	32/58/-88	208/32/-94	67	85	15	5
12	21-10-2010	2:49:55	-73.726	-34.737	10	7,42E + 27	5.90	12/54/-112	227/42/-62	80	42	58	3
13	13-12-2010	18:51:04	-73.080	-33.989	6	4,98E + 26	5.10	63/59/-64	200/40/-125	78	78	22	3

more than three stations to obtain robust solutions, as done in the subduction zone in Japan (e.g. Fukuyama and Dreger, 2000; Kubo et al., 2002). In our analysis, except for one event with a low VR, the regional moment tensors were obtained using at least more than three stations.

For the large outer trench slope event,  $M_w$  7.4, the overlapping seismic waves issue was counterbalanced by using regional stations and a

specific bandpass filter. Unfortunately, it was not possible to invert the coseismic slip distribution or the source time function for this event. The rupture fault plane shown in Fig. 6 was estimated based on standard scaling laws for intraplate earthquakes, however with the seismological dataset available the along-dip slipped zone during the earthquake is not well resolved.

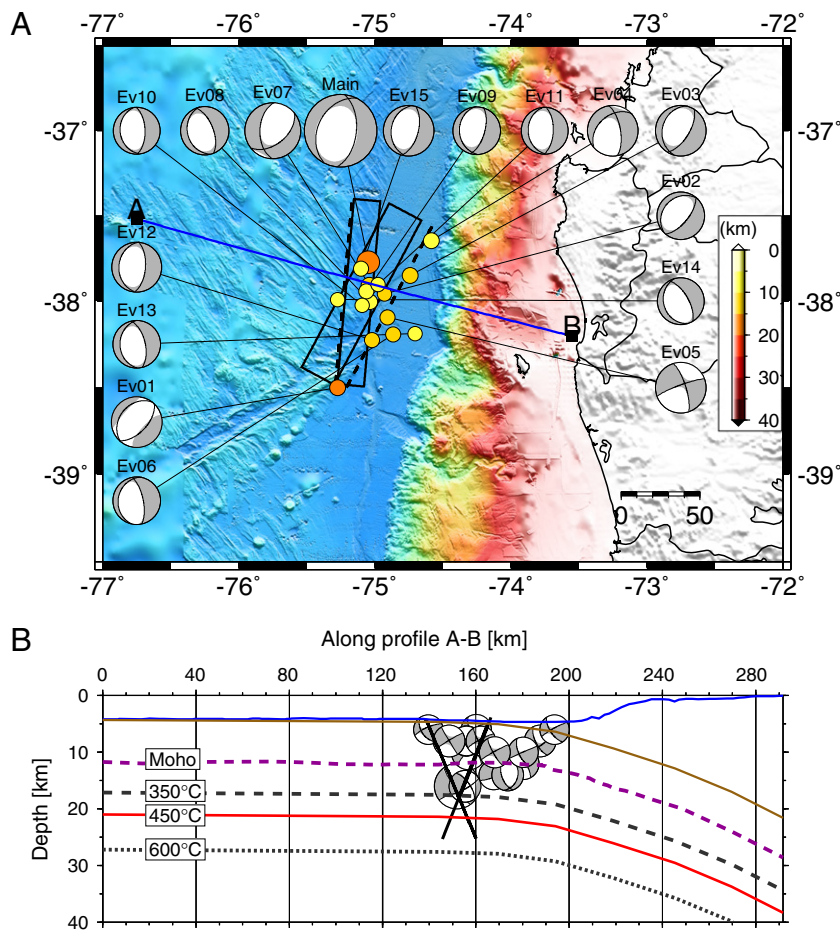


**Fig. 6.** Regional seismic moment tensors modeled in this study for the outer rise events located in the southern region of the study area. (A) High resolution bathymetric map and spatial distribution of all regional moment tensor solutions, where colored circles correspond to its epicenter location. For the largest outer trench slope event,  $M_w$  7.4, we estimate the two possible rupture fault planes (solid black line) assuming a rectangular fault. The dashed and solid dark lines are the fault trace and fault edges projected to the free surface, respectively. Color bar represents the best source depth estimated during the inversion. (B) Cross-section A-B shows the best source depth (centroid) estimated in this study and dark oblique lines are the two nodal fault planes estimated along dip. Brown line is the top of the oceanic subducting slab, purple dashed line is the Moho discontinuity, and blue solid line is the bathymetry. The black dashed, red solid and black dotted lines are the 350 °C, 450 °C and 600 °C isotherms, respectively, computed for the subducting oceanic slab based on the cooling of a semi-infinite half-space model (e.g. Turcotte and Schubert, 1982). The estimated depths for the isotherms are also consistent with the thermal model developed by Voelker et al. (2011) off south central Chile.

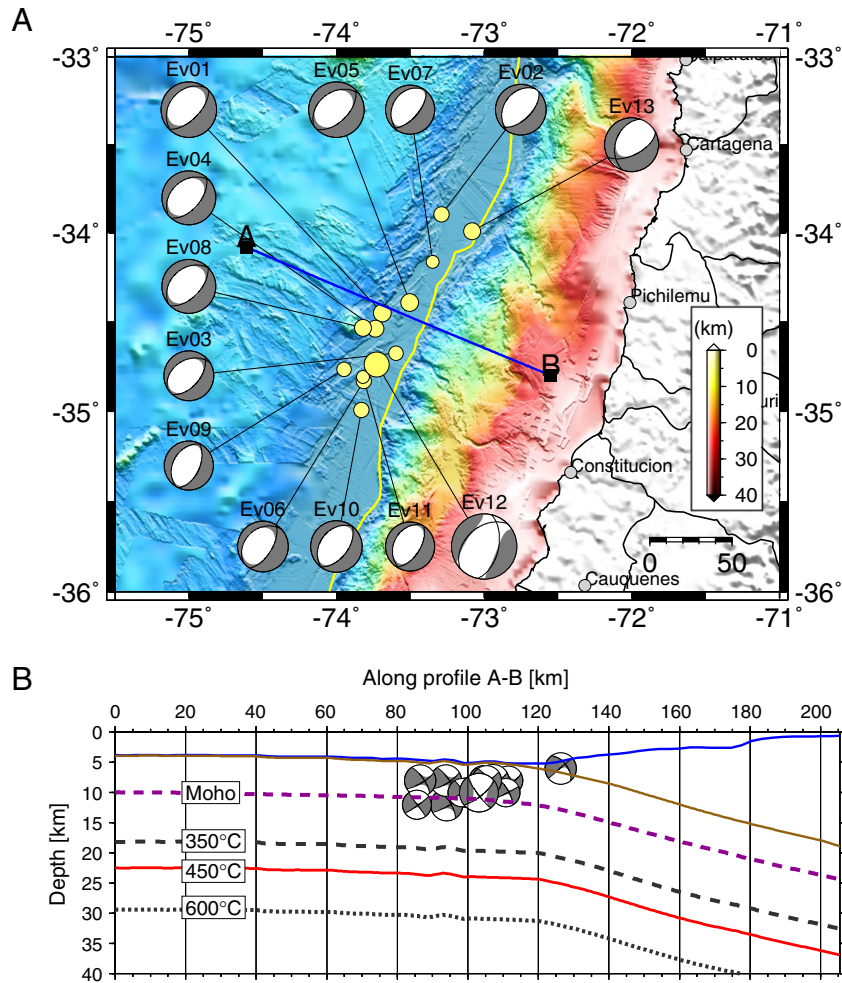


**Fig. 7.** Regional seismic moment tensors modeled in this study for the outer rise events located at the northern region of the study area. (A) High resolution bathymetric map and spatial distribution of all regional moment tensor solutions computed in this study, where colored circles correspond to its epicenter location. Yellow line is the trench axis and the colorbar represents the best source depth (centroid) estimated from the inversion. (B) Cross-section A–B shows the best source depth estimated in this study. Brown line is the top of the oceanic subducting slab, purple dashed line is the Moho discontinuity, and blue solid line is the bathymetry (Moscoso and Contreras-Reyes, 2012). The black dashed, red lines, and black dotted lines are the 350 °C, 450 °C and 600 °C isotherms, respectively, computed for the subducting oceanic slab based on the cooling of a semi-infinite half-space model (e.g. Turcotte and Schubert, 1982).

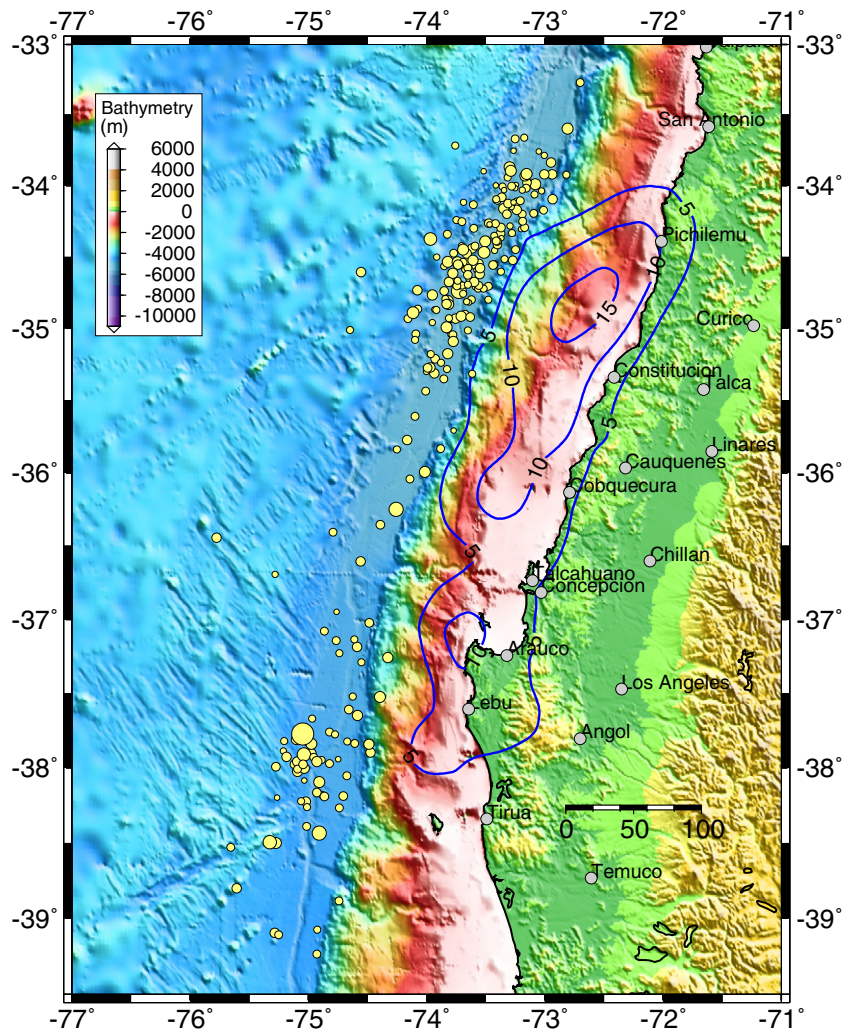
**5.2. Influence of the coseismic slip of the Maule megathrust earthquake on outer rise seismicity and adjacent areas**

Fig. 8 shows the coseismic slip model of Moreno et al. (2012) and the outer rise seismicity triggered by the Maule event. Most of the outer rise events (~70%) lie just west of the northern Maule asperity, which has the maximum peak-slip of ~15 m (Lorito et al., 2011; Vigny et al., 2011; Moreno et al., 2012). The observed outer rise seismicity can be seen as a direct consequence of the stress transferred from the large coseismic slip of the northern asperity of the Maule event. Interestingly, the massive northern cluster of outer rise events is located within 50 km from the trench axis, which is the zone of maximum bending moment according to 3D flexure modeling of the oceanic Nazca plate (Manríquez et al., 2014).

On the other hand, westward of the region of low coseismic slip (in the epicentral region) between 36°S and 37°S, the outer rise of the oceanic Nazca plate presents little intraplate seismicity supporting the idea that regions of low coseismic slip transfer little stress to the downgoing plate (Christensen and Ruff, 1988; Dmowska and Lovison, 1992). However, almost no outer rise seismic activity with events of  $M_w > 4.0$  is observed in the outer rise west of the southern Maule asperity (Fig. 8), even though ~10 m of slip is thought to have occurred on the megathrust here (Lorito et al., 2011; Moreno et al., 2012).

Instead, most of the outer rise seismicity is concentrated southwest of the southern Maule asperity, and some of the events are aligned with the Mocha FZ.

A possible mechanism explaining the asymmetry of the outer rise seismic activity triggered by the southern asperity of the Maule earthquake is the migration of the intraplate seismicity to regions of pre-existing large intraplate faults and weakness. A natural candidate is the Mocha FZ, which hosts an uppermost oceanic mantle hydrofractured up to depths of ~20 km according to seismic constraints (Contreras-Reyes et al., 2008). Fig. 6A shows that the largest extensional event ( $M_w$  7.4) occurred just 40 km north of the Mocha FZ, and the associate aftershocks sequence apparently migrated towards the trenchward part of the Mocha FZ. Almost all events were extensional and at depths shallower than 20 km (isotherm of 400–450 °C, Fig. 6B), and hence consistent with the proposed estimate for the depth of the neutral plane (~20 km) by Seno and Yamanaka (1996). One strike-slip event located near the Mocha FZ suggests the reactivation of the fossil transform fault. This interpretation is also supported not only by the large spatial concentration of outer rise events, but also by the diversity in strike direction of the outer rise extensional events. Nevertheless, these events are concentrated at the trenchward part of the outer rise, where bending tensional plates are larger, rather than elsewhere along the fracture zone.



**Fig. 8.** Outer rise events located by the NEIC (yellow circles) that followed the 2010,  $M_w$  8.8, Maule earthquake, in the period 27-02-2010 to 31-12-2013, including the large outer trench slope  $M_w$  7.4 earthquake. Circles are scaled to event magnitude. Blue line contours represent the amplitude of the coseismic slip of the 2010,  $M_w$  8.8, Maule megathrust earthquake (Moreno et al., 2012).

Reactivation of fossil transform faults as a consequence of megathrust earthquakes has also been reported off Sumatra with a sequence of large strike-slip earthquakes of  $M_w > 8.4$  (Meng et al., 2012). Coulomb stress change calculations show that the coseismic slips of the  $M_w$  9.2, 2004, Sumatra–Andaman megathrust earthquake can promote oceanic left-lateral strike-slip earthquakes on pre-existing meridian-aligned fault planes (Delescluse et al., 2012). However, there is not much outer rise seismicity reported off Sumatra, where apparently most of the intraplate seismicity is concentrated on the pre-existing meridian-aligned fault planes (some located several hundred of kilometers from the Sumatra trench). In contrast, intraplate seismicity boosted by the Maule megathrust earthquake includes both outer rise seismicity and the reactivation of a paleo-transform fault as shown in Fig. 1. Intraplate stresses inherited from the Maule main shock were not strong enough to re-activate the Mocha FZ further seaward, and most of the seismicity was concentrated in the outer rise region. Nonetheless, intraplate events with a significant strike-slip component support the idea of reactivation of the paleo-transform fault.

### 5.3. Lithospheric strength and tectonic implications

The age of the oceanic Nazca plate is estimated to be  $\sim 34$  and  $\sim 30$  Ma in the region of the northern and southern intraplate clusters, respectively (Tebbens et al., 1997). In Fig. 9, we show the yield strength

envelope of the oceanic lithosphere along with the depth distribution for an oceanic plate representative of the studied region with a plate age of 32 Ma. Here the lithospheric strength is calculated by combining Byerlee's frictional sliding rule at shallow depth, and the rheology for wet olivine for the ductile portion (Kohlstedt et al., 1995). A geotherm for a 32 million year old lithosphere and a strain rate of  $10^{-15} \text{ s}^{-1}$  is assumed. The brittle–ductile transition for this 32 Myr old oceanic lithosphere occurs at  $\sim 21$  km in the tensional regime, which is roughly the depth limit for the largest  $M_w$  7.4 outer rise event or overall outer rise events in the region (Fig. 9). The consistency between the strength envelope and the maximum depths of intraplate tensional events suggests that the earthquake sequence ruptured through the entire brittle part of the oceanic lithosphere. The brittle–ductile transition is strongly controlled by the thermal state of the oceanic plate, and it is a natural rheological boundary preventing deeper rupture for intraplate events. Interestingly, and particularly for this case of a 32 Ma oceanic plate, the brittle–ductile transition depth is roughly coincident with the  $450^\circ\text{C}$  isotherm, which is suggested as the depth for the tension/compression transition (Seno and Yamanaka, 1996). Consistently, the tension/compression transition or neutral surface is also another deep limit for tensional faulting.

Failure of the whole brittle upper part of the oceanic lithosphere is also consistent with previous studies that show that the oceanic Nazca plate in the region is highly fractured as a consequence of

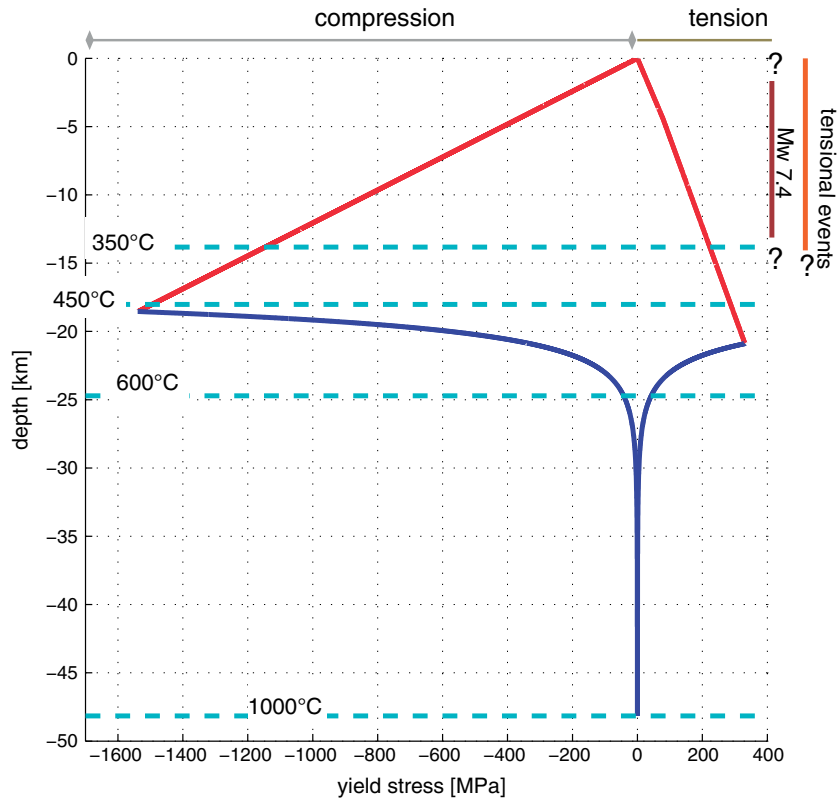


**Fig. 9.** Strength envelope for an oceanic lithosphere 32 Myr old. Stress differences or yield stress are limited at the top of the plate by frictional sliding rule according to Byerlee's frictional sliding rule (red curve). Yield stress is limited at the base of the plate by steady state creep, which depends on the cube of the stress and exponentially on temperature (e.g. Kohlstedt et al., 1995). Isotherms were computed based on the cooling of a semi-infinite half-space model (e.g. Turcotte and Schubert, 1982). The depth range for the outer rise events is delimited by the orange straight line. The brown orange straight line denotes the depth range of the largest  $M_w$  7.4 outer rise. Please note that depths are measured from the seafloor. In contrast, for Figs. 6 and 7, depths are measured from the sea level.

bending related faulting (Contreras-Reyes et al., 2008; Moscoso and Contreras-Reyes, 2012). Active seismic investigations have found evidence for active deformation on north–south trending faults, probably resulting from the reactivation of the tectonic fabric of the seafloor (Contreras-Reyes et al., 2008; Moscoso and Contreras-Reyes, 2012). In particular, at  $\sim 36.5^\circ\text{S}$  and  $\sim 38.5^\circ\text{S}$ , Diaz-Naveas (1999) and Grevenmeyer et al. (2005) imaged bending faults with seismic reflection data that cut at least  $\sim 6$  km into the uppermost mantle. This mechanism has been proposed to drive hydration of the upper part of the oceanic lithosphere and consequently mantle serpentinization (see for instance Faccenda, 2014 for a review). Owing to the large number and great magnitude of outer rise events boosted by the Maule megathrust earthquake, water percolation into the upper mantle is expected to be more efficient during the co-seismic phase of large megathrust earthquakes (Moscoso and Contreras-Reyes, 2012).

## 6. Conclusions

We analyzed the outer rise events triggered after the 2010 Maule  $M_w$  8.8 megathrust earthquake that occurred in south-central Chile and discuss its relationship to the subduction process and mechanisms responsible for triggering such events. Our analysis focused on computing regional seismic moment tensors for a large set of outer rise events (29 events with  $M_w \geq 4.5$ ) by inverting 3-component broadband regional waveforms.

We analyzed the largest outer rise event triggered by the Maule mainshock. This outer trench slope event,  $M_w$  7.4, nucleated just 1.5 h after the mainshock, had a normal fault mechanism and centroid depth of about 16 km; all these characteristics strongly suggest that it was triggered as a direct response to the stress transfer from the slipped

megathrust fault to the outer trench slope zone in the very early post-seismic phase. This event was located off shore the southern edge of the mainshock rupture area, near the oceanic Mocha FZ.

Intense outer rise seismicity following the 2010 Maule earthquake was spatially distributed in two main zones. The northern zone, offshore the largest slip patch during the Maule earthquake, concentrated most of the outer rise seismicity. Offshore the southern edge of the Maule rupture area, a second cluster of outer rise seismicity was triggered with fewer events compared to the north.

According to our moment tensor solutions, most of the intraplate events were tensional, with centroid depths located in the upper 20 km of the subducting oceanic plate; however, the northern and southern outer rise events present distinctive characteristics. Similar focal mechanisms were obtained for all outer rise events in the northern zone, which are characterized by an extensional sense of faulting, same strike angle (in average  $38^\circ$ , or  $220^\circ$ , for either one or the other nodal plane) and present little fluctuation in terms of magnitudes and centroid depths.

In contrast, even if most of the southern outer rise events were associated with extensional faulting, a few events present a different focal mechanism. The centroid depth of events varies from 5 to 20 km depth, and present comparable magnitudes. The majority of events strike nearly parallel to the trench axis, except four events with average strike of  $N20^\circ\text{W}$ . Several large events nucleated near the trenchward part of the oceanic Mocha FZ, and some of these events have a significant strike–slip component aligned with this oceanic feature.

The predicted yield strength envelope for 32 Ma oceanic lithosphere suggests that intraplate tensional events rupture through the entire brittle part of the oceanic lithosphere up to depths of 20 km.

## Acknowledgments

We thank the IRIS data center and NEIC for providing easy access to worldwide broadband waveforms. Some figures were drawn with the software package Generic Mapping Tools (GMT) v4.5 (Wessel and Smith, 1998). Signal processing was done using Seismic Analysis Code, SAC (Goldstein et al., 2003). We gratefully acknowledge the support of the *Chilean Comisión Nacional de Investigación Y Tecnología* (CONICYT) under the grant USA2012-001 (Cooperación Chile-EEUU). We thank the Editor, and two anonymous reviewers for suggestions and comments that improved the manuscript. We kindly thank Dr. Anne Trehu for helpful comments and for proofreading the manuscript. We also thank Hiroo Kanamori for useful comments and suggestions.

## References

- Ammon, C.J., Kanamori, H., Lay, T., 2008. A great earthquake doublet and seismic stress transfer cycle in the central Kuril Islands. *Nat. Lett.* 451, 561–565. <http://dx.doi.org/10.1038/nature06521>.
- Asano, Y., Saito, T., Ito, Y., Shiomi, K., Hirose, H., Matsumoto, T., Aoi, S., Hori, S., Sekiguchi, S., 2011. Spatial distribution and focal mechanisms of aftershocks of the 2011 off the Pacific coast of Tohoku earthquake. *Earth Planets Space* 63 (7), 669–673. <http://dx.doi.org/10.5047/eps.2011.06.016>.
- Campos, J., Hatzfeld, D., Madariaga, R., Lopez, G., Kausel, E., Zollo, A., Barrientos, S., Lyon-Caen, H., 2002. The 1835 seismic gap in south central Chile. *Phys. Earth Planet. Inter.* 132, 177–195.
- Chapple, W.M., Forsyth, D.W., 1979. Earthquakes and bending of plates at trenches. *J. Geophys. Res.* 84 (B12), 6729–6749. <http://dx.doi.org/10.1029/JB084iB12p06729>.
- Christensen, D.H., Ruff, L.J., 1988. Seismic coupling and outer rise earthquakes. *J. Geophys. Res.* 93 (B11), 13421–13444. <http://dx.doi.org/10.1029/JB093iB11p13421>.
- Clouard, V., Campos, J., Lemoine, A., Perez, A., Kausel, E., 2007. Outer rise stress changes related to the subduction of the Juan Fernandez Ridge, central Chile. *J. Geophys. Res.* 112, B05305. <http://dx.doi.org/10.1029/2005JB003999>.
- Contreras-Reyes, E., Grevemeyer, I., Flueh, E.R., Reichert, C., 2008. Upper lithospheric structure of the subduction zone offshore of southern Arauco peninsula, Chile, at ~38°S. *J. Geophys. Res.* 113, B07303. <http://dx.doi.org/10.1029/2007JB005569>.
- Delescluse, M., Chamot-Rooke, N., Cattin, R., Fleitout, L., Trubienko, O., Vigny, C., 2012. April 2012 intra-oceanic seismicity off Sumatra boosted by the Banda-Aceh megathrust. *Nature* 490, 240–244. <http://dx.doi.org/10.1029/2012nature11520>.
- Delouis, B., Nocquet, J.-M., Vallée, M., 2010. Slip distribution of the February 27, 2010 Mw = 8.8 Maule earthquake, central Chile, from static and high-rate GPS, InSAR, and broadband teleseismic data. *Geophys. Res. Lett.* 37, L17305. <http://dx.doi.org/10.1029/2010GL043899>.
- Diaz-Naveas, J.L., 1999. Sediment subduction and accretion at the Chilean convergent margin between 35 and 40S. Ph.D. thesis. Univ. of Kiel, Kiel, Germany.
- Dmowska, R., Lovison, L., 1992. Influence of asperities along subduction interfaces on the stressing and seismicity of adjacent areas. *Tectonophysics* 211, 23–43.
- Dmowska, R., Rice, J.R., Lovison, L.C., Josell, D., 1988. Stress transfer and seismic phenomena in coupled subduction zones during the earthquake cycle. *J. Geophys. Res.* 93 (B7), 7869–7884. <http://dx.doi.org/10.1029/JB093iB07p7869>.
- Dmowska, R., Zheng, G., Rice, J.R., 1996. Seismicity and deformation at convergent margins due to heterogeneous coupling. *J. Geophys. Res.* 101 (B2), 3015–3029. <http://dx.doi.org/10.1029/95JB03122>.
- Dreger, D.S., 2003. TDMT\_INV: time domain seismic moment tensor INVersion. *Int. Handb. Earthq. Eng. Seismol.* 81B, 1627.
- Faccenda, M., 2014. Water in the slab: a trilogy. *Tectonophysics* <http://dx.doi.org/10.1016/j.tecto.2013.12.020>.
- Fariás, M., Comte, D., Roecker, S., Carrizo, D., Pardo, M., 2011. Crustal extensional faulting triggered by the 2010 Chilean earthquake: the Pichilemu Seismic Sequence. *Tectonics* 30, TC6010. <http://dx.doi.org/10.1029/2011TC002888>.
- Fritz, H.M., Petroff, C.M., Catalan, P.A., Cienfuegos, R., Winckler, P., Kalligeris, N., Weiss, R., Barrientos, S.E., Meneses, G., Valderas-Bermejo, C., Ebeling, C., Papadopoulos, A., Contreras, M., Almar, R., Dominguez, J.C., Synolakis, C.E., 2011. Field survey of the 27 February 2010 Chile tsunami. *Pure Appl. Geophys.* 168, 1989–2010. <http://dx.doi.org/10.1007/s00024-011-0283-5>.
- Fukuyama, E., Dreger, D., 2000. Performance test of an automated moment tensor determination system for the future “Tokai” earthquake. *Earth Planets Space* 52, 383–392.
- Goldstein, P., Dodge, D., Firpo, M., Minner, L., 2003. SAC2000: signal processing and analysis tools for seismologists and engineers. In: Lee, W.H.K., Kanamori, H., Jennings, P.C., Kisslinger, C. (Eds.), *IASPEI International Handbook of Earthquake and Engineering Seismology*. Academic Press, Amsterdam & Boston.
- Grevemeyer, I., Kaul, N., Diaz-Naveas, J.L., Villinger, H., Ranero, C.R., Reichert, C., 2005. Heat flow and bending-related faulting at subduction trenches: Case studies offshore of Nicaragua and central Chile. *Earth Planet. Sci. Lett.* 236, 238–248. <http://dx.doi.org/10.1016/j.epsl.2005.04.048>.
- Hayes, G.P., Bergman, E., Johnson, K.L., Benz, H.M., Brown, L., Meltzer, A., 2013. Seismotectonic framework of the February 27, 2010 Mw 8.8 Maule, Chile earthquake sequence. *Geophys. J. Int.* 195 (2), 1034–1051. <http://dx.doi.org/10.1093/gji/ggt238>.
- Kanamori, H., 1971. Seismological evidence for a lithospheric normal faulting — the Sanriku earthquake of 1933. *Phys. Earth Planet. Inter.* 4, 289–300.
- Khazaradze, G., Klotz, J., 2003. Short- and long-term effects of GPS measured crustal deformation rates along the south central Andes. *J. Geophys. Res.* 108, 2289. <http://dx.doi.org/10.1029/2002JB001879>.
- Kohlstedt, D.L., Evans, B., Mackwell, S.J., 1995. Strength of the lithosphere — constraints imposed by laboratory experiments. *J. Geophys. Res.* 100 (B9), 17,587–17,602.
- Korrat, I., Madariaga, R., 1986. Rupture of the Valparaiso (Chile) gap from 1971 to 1985. In: Das, S., Boatwright, J., Scholz, C. (Eds.), *Earthquake Source Mechanics*, Maurice Ewing Ser. vol. 6. AGU, Washington, D. C., pp. 247–258.
- Kubo, A., Fukuyama, E., Kawai, H., Nonomura, K., 2002. NIED seismic moment tensor catalogue for regional earthquakes around Japan: quality test and application. *Tectonophysics* 356 (1–3), 23–48. [http://dx.doi.org/10.1016/S0040-1951\(02\)00375-X](http://dx.doi.org/10.1016/S0040-1951(02)00375-X).
- Lange, D., Tilmann, F., Barrientos, S., Contreras-Reyes, E., Methe, P., Moreno, M., Heit, B., Agurto, H., Bernard, P., Vilotte, J.-P., Beck, S., 2012. Aftershock seismicity of the 27 February 2010 Mw 8.8 Maule earthquake rupture zone. *Earth Planet. Sci. Lett.* 317–318C, 413–425. <http://dx.doi.org/10.1016/j.epsl.2011.11.034>.
- Lay, T., Ammon, C.J., Kanamori, H., Rivera, L., Koper, K.D., Hutko, A.R., 2010. The 2009 Samoa–Tonga great earthquake triggered doublet. *Nature* 466, 964–968. <http://dx.doi.org/10.1038/nature09214>.
- Lay, T., Ammon, C.J., Kanamori, H., Kim, M.J., Xue, L., 2011. Outer trench-slope faulting and the 2011 Mw 9.0 off the Pacific coast of Tohoku earthquake. *Earth Planets Space* 63, 713–718. <http://dx.doi.org/10.5047/eps.2011.05.006>.
- Lomnitz, C., 2004. Major earthquakes of Chile: a historical survey, 1535–1960. *Seismol. Res. Lett.* 75 (3), 368–378. <http://dx.doi.org/10.1785/gssrl.75.3.368>.
- Lorito, S., Romano, F., Atzori, S., Tong, X., Avallone, A., McCloskey, J., Cocco, M., Boschi, E., Piatanesi, A., 2011. Limited overlap between the seismic gap and coseismic slip of the great 2010 Chile earthquake. *Nat. Geosci.* 4, 173–177. <http://dx.doi.org/10.1038/ngeo1073>.
- Madariaga, R., Métois, M., Vigny, C., Campos, J., 2010. Central Chile finally breaks. *Science* 328 (5975), 181–182. <http://dx.doi.org/10.1126/science.1189197>.
- Manríquez, P., Contreras-Reyes, E., Osse, A., 2014. Lithospheric 3D flexure modelling seaward of the oceanic plate seaward of the trench using variable elastic thickness. *Geophys. J. Int.* 196, 681–693. <http://dx.doi.org/10.1093/gji/ggt464>.
- Meng, L., Ampuero, J.-P., Stock, J., Duputel, Z., Luo, Y., Tsai, V.C., 2012. Earthquake in a Maze: Compressional Rupture Branching During the 2012 Mw 8.6 Sumatra Earthquake. *Science* 337 (6095), 724–726. <http://dx.doi.org/10.1126/science.1224030>.
- Moreno, M., Melnick, D., Rosenau, M., Baez, J., Klotz, J., Oncken, O., Tassara, A., Chen, J., Bataille, K., Bevis, M., Socquet, A., Bolte, J., Vigny, C., Brooks, B., Ryder, I., Grund, V., Smalley, B., Carrizo, D., Bartsch, M., Hase, H., 2012. Toward understanding tectonic control on the Mw 8.8 2010 Maule Chile earthquake. *Earth Planet. Sci. Lett.* 321–322, 152–165. <http://dx.doi.org/10.1016/j.epsl.2012.01.006>.
- Moscoco, E., Contreras-Reyes, E., 2012. Outer rise seismicity related to the Maule, Chile 2010 megathrust earthquake and hydration of the incoming oceanic lithosphere. *Andean Geol.* 39 (3), 564–572. <http://dx.doi.org/10.5027/andgeoV39n3-a12>.
- Obana, K., Fujie, G., Takahashi, T., Yamamoto, Y., Nakamura, Y., Kodaira, S., Takahashi, N., Kaneda, Y., Shinohara, M., 2012. Normal-faulting earthquakes beneath the outer slope of the Japan Trench after the 2011 Tohoku earthquake: implications for the stress regime in the incoming Pacific plate. *Geophys. Res. Lett.* 39, L00G24. <http://dx.doi.org/10.1029/2011GL050399>.
- Pasyanos, M.E., Dreger, D.S., Romanowicz, B., 1996. Toward real-time estimation of regional moment tensors. *Bull. Seismol. Soc. Am.* 86 (5), 1255–1269.
- Rietbrock, A., Ryder, I., Hayes, G., Haberland, C., Comte, D., Roecker, S., Lyon-Caen, H., 2012. Aftershock seismicity of the 2010 Maule Mw = 8.8, Chile, earthquake: correlation between co-seismic slip models and aftershock distribution? *Geophys. Res. Lett.* 39, L08310. <http://dx.doi.org/10.1029/2012GL051308>.
- Ritsema, J., Lay, T., 1995. Long-period regional wave moment tensor inversion for earthquakes in the western United States. *J. Geophys. Res.* 100 (B6), 9853–9864. <http://dx.doi.org/10.1029/95JB00238>.
- Ruegg, J.C., Rudloff, A., Vigny, C., Madariaga, R., de Chabaliere, J.B., Campos, J., Kausel, E., Barrientos, S., Dimitrov, D., 2009. Interseismic strain accumulation measured by GPS in the seismic gap between Constitución and Concepción in Chile. *Phys. Earth Planet. Inter.* 175, 78–85.
- Ruiz, J.A., Hayes, G.P., Carrizo, D., Kanamori, H., Socquet, A., Comte, D., 2014. Seismological analyses of the 2010 March 11, Pichilemu, Chile Mw 7.0 and Mw 6.9 coastal intra-plate earthquakes. *Geophys. J. Int.* 197 (1), 414–434. <http://dx.doi.org/10.1093/gji/ggt513>.
- Ryder, I., Rietbrock, A., Kelson, K., Burgmann, R., Floyd, M., Socquet, A., Vigny, C., Carrizo, D., 2012. Large extensional aftershocks in the continental forearc triggered by the 2010 Maule earthquake, Chile. *Geophys. J. Int.* <http://dx.doi.org/10.1111/j.1365-246X.2011.05321.x>.
- Saikia, C.K., 1994. Modified frequency–wavenumber algorithm for regional seismograms using Filon’s quadrature: modelling of Lg waves in eastern North America. *Geophys. J. Int.* 118, 142–158. <http://dx.doi.org/10.1111/j.1365-246X.1994.tb04680.x>.
- Seno, T., Yamanaka, Y., 1996. Double seismic zones, compressional deep trench-outer rise events and superplumes. In: Bebout, G., et al. (Eds.), *Subduction: Top to Bottom*. *Geophys. Monogr. Ser.* vol. 96. AGU, Washington, D. C., pp. 347–355.
- Spence, W., 1986. The 1977 Sumba Earthquake Series: Evidence for Slab Pull Force Acting at a Subduction Zone. *J. Geophys. Res.* 91 (B7), 7225–7239. <http://dx.doi.org/10.1029/JB091iB07p7225>.
- Strasser, F.O., Arango, M.C., Bommer, J.J., 2010. Scaling of the source dimensions of interface and intraslab subduction-zone earthquakes with moment magnitude. 81 (No. 6), 941–950. <http://dx.doi.org/10.1785/gssrl.81.6.941>.
- Taylor, M.A., Zheng, G., Rice, J.R., Stuart, W.D., Dmowska, R., 1996. Cyclic stressing and seismicity at strongly coupled subduction zones. *J. Geophys. Res.* 101 (B4), 8363–8381. <http://dx.doi.org/10.1029/95JB03561>.

- Tebbens, S.F., Cande, S.C., Kovacs, L., Parra, J.C., LaBrecque, J.L., Vergara, H., 1997. The Chile ridge: a tectonic framework. *J. Geophys. Res.* 102, 12,035–12,060. <http://dx.doi.org/10.1029/96jB02581>.
- Turcotte, D., Schubert, G., 1982. *Geodynamics—Applications of Continuum Physics to Geological Problems*. John Wiley, Hoboken, N. J. (464 pp.).
- Vargas, G., Fariás, M., Carretier, S., Tassara, A., Baize, S., Melnick, D., 2011. Coastal uplift and tsunami effects associated to the 2010 Mw 8.8 Maule earthquake in central Chile. *Andean Geol.* 38 (1), 219–238.
- Vigny, C., et al., 2011. The 2010 Mw 8.8 Maule megathrust earthquake of central Chile, monitored by GPS. *Science* 332, 1417. <http://dx.doi.org/10.1126/science.1204132>.
- Voelker, D., Grevemeyer, I., Stipp, M., Wang, K., He, J., 2011. Thermal control of the seismogenic zone of southern central Chile. *J. Geophys. Res.* 116. <http://dx.doi.org/10.1029/2011jB008247>.
- Wessel, P., Smith, W.H.F., 1998. New, improved version of generic mapping tools released. *EOS Trans. Am. Geophys. Union* 79 (47), 579.
- Yue, H., Lay, T., Koper, K.D., 2012. En échelon and orthogonal fault ruptures of the 11 April 2012 great intraplate earthquakes. *Nature* 490, 245–249. <http://dx.doi.org/10.1038/nature11492>.